# All-Optical High-Resolution Nanopatterning and 3D Suspending of Graphene

**Rainer J. Stöhr,* Roman Kolesov, Kangwei Xia, and Jörg Wrachtrup**

3. Physikalisches Institut, Universität Stuttgart, 70550 Stuttgart, Germany and Stuttgart Research Center of Photonic Engineering (SCoPE), 70569 Stuttgart, Germany

**ABSTRACT** We introduce a laser-based technique capable of both imaging and patterning graphene with high spatial resolution. Both tasks are performed *in situ* using the same confocal microscope. Imaging graphene is based on the recombination of a laser-created electron–hole plasma yielding to a broadband up- and down-converted fluorescence. Patterning is due to burning graphene by local heating causing oxidation and conversion into $CO_2$. By shaping the laser beam profile using 1D phase-shifting plates and 2D vortex plates we can produce graphene dots below 100 nm in diameter and graphene nanoribbons down to 20 nm in width. Additionally, we demonstrate that this technique can also be applied to freely suspended graphene resulting in freely suspended graphene nanoribbons. We further present a way of freely hanging graphene vertically and imaging it in 3D. Taking advantage of having vertically hanging graphene for the first time, we measure the out-of-plane anisotropy of the upconversion fluorescence.

**KEYWORDS:** graphene · freely suspended graphene · graphene nanoribbon · laser lithography · laser etching

Owing to its very unique properties graphene became a playground for studying fundamental aspects of relativistic charge carries confined in 2D.[1−4] Even though the first milestone experiments were performed on graphene bulk samples, soon graphene nanoribbons (GNRs) attracted significant attention.[5−7] Other than in bulk graphene, GNRs exhibit a band gap which increases with decreasing width of the GNRs due to the lateral confinement of charge carriers.[8,9] Together with the high charge carrier mobility this makes GNRs a promising material for graphene-based electronic devices.[10] Additionally, having graphene freely suspended and therefore avoiding any influence from the substrate was another crucial step in exploring graphenes full capabilities.[11,12] However, until now, shaping graphene into GNRs is mostly done by electron-beam lithography combined with plasma etching[13] which requires rather excessive multistep processing including wet-chemical treatment and can therefore not be applied to freely suspended GNRs. Here, we show an all-optical alternative of producing GNRs which overcomes those drawbacks while still being capable of producing GNRs down to 20 nm width which can also be applied to freely suspended graphene resulting in freely suspended GNRs of controllable width. Finally, we demonstrate a way of hanging graphene vertically (perpendicular to the substrate) which to our knowledge has also not been reported until now. By the example of laser induced upconverted graphene fluorescence[14,15] we highlight how freely hanging graphene can be used to measure the out-of-plane anisotropy of optical effects by turning linear laser polarization perpendicular to graphene.

The two underlying principles for this study are the imaging of graphene by upconverted luminescence and local removal of graphene using high power pulsed laser irradiation. It has been shown that upconversion imaging is a powerful tool for mapping single- and multilayer flakes on various substrates and to determine the exact shape and number of layers.[14] By exciting graphene with pico- or femtosecond laser pulses a local high density plasma is created due to a high number of excited electron hole pairs. Unlike in the case of continuous wave excitation this high density leads to scattering between the charge carriers.

Opposite to the case of massive particles, the scattering of initially monoenergetic massless charge carriers results in an efficient energy exchange between them and, consequently, to a broad energy distribution among them.[14] The recombination of such a thermalized electron hole plasma presents itself in a broad luminescence spectrum centered around the excitation energy and reaching several thousands of wavenumbers higher and lower in energy (see Figure 1). Since the scattering probability is proportional to the square of the plasma density the luminescence intensity

* Address correspondence to r.stoehr@physik.uni-stuttgart.de.

Received for review April 1, 2011 and accepted May 19, 2011.

**Published online May 19, 2011**
**10.1021/nn201226f**

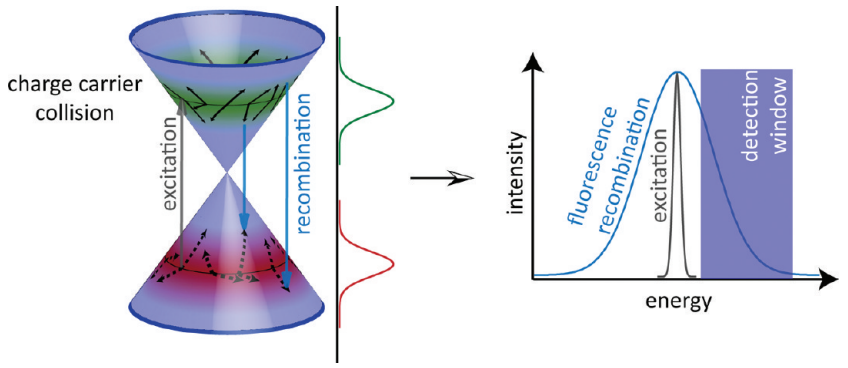


**Figure 1. Schematic representation of the 2D dispersion relation of graphene. The gray arrow shows the optical excitation of initially monoenergetic electron−hole pairs. Collisions lead to a broadening of the energy distribution as shown by the green and red curves. Recombination of shifted electron hole pairs leads to a broad fluorescence centered around the excitation energy.**

is proportional to the square of the laser intensity. Using the upconverted part of this luminescence for imaging graphene has several advantages compared to other imaging techniques. Since the detected signal is higher in energy than the excitation, it is a background-free technique because of the absence of the fluorescence from the substrate or other impurities. Also, because of the high intensity of the emission and a strong dependence on the number of layers, a high image contrast can be achieved. The nonlinear nature of the luminescence further improves the imaging resolution. Using pulsed IR illumination makes it possible both to image and shape graphene in one seamless operation. In the regime of low laser intensity, graphene can be safely imaged as described above without introducing any defects. However, in the high intensity regime, graphene is locally removed by the laser. The efficiency of this process was measured by recording the upconversion intensity for different laser powers as a function of time after the laser is switched on. The rate plotted in Figure 2 is the inverse of the time needed until the upconversion intensity reached one-half of the original value for undamaged graphene. From the left inset it can be seen that in the imaging regime the upconversion intensity remains stable even for 100 s verifying that no damage has been inflicted during that time. (Note that for imaging graphene each point is exposed to the laser only for a few of tens of milliseconds total.) However, in the shaping regime, graphene is efficiently removed already after a few milliseconds as shown in the right inset. The decay of the upconversion intensity does not follow a simple exponential law but shows quite complicated temporal evolution. Also, it was observed that by pumping the sample chamber and reducing the atmospheric pressure by a factor of 50 the time needed for burning increased by the same factor. This suggests that graphene heated by the laser beam becomes involved in a chemical reaction with atmospheric oxygen and forms $CO_2$. This hypothesis validates the term "burning" used previously. The temporal evolution of the burning process might be rather complicated and can include several stages. At the first stage, the pristine undamaged graphene can efficiently drain out the laser-induced heat due to its high heat conductivity.[16] However, some carbon atoms are stochastically being extracted from the crystal lattice to form $CO_2$. This process destroys the integrity of the graphene lattice and reduces the heat conductivity. This, in turn, increases the probability for each particular carbon atom to be oxidized. Both heating and lattice destruction result in an avalanche process of burning. Even though the correct description of graphene burning would require numerical simulation of the dynamics of the lattice subject to laser heating, the process described above is the most probable qualitative scenario. One important aspect is, however, that this effect appears to be a very local phenomenon despite very high in-plane heat conductivity of pristine graphene. It can therefore be used to pattern graphene with very high spatial resolution. Since the heat dissipation is also influenced by the thermal coupling to the surrounding it could be observed that the intensity needed for burning differs depending on the substrate material. However, nanoshaping of graphene by local laser induced burning can be done on arbitrary substrates and can even be applied to freely suspended graphene. A simplified semiempirical model of producing a freely suspended GNR will be discussed below to give an estimate on the smallest feasible feature size.

## RESULTS AND DISCUSSION

As a first step, we show how graphene can be imaged using upconverted luminescence and subsequently patterned *in situ* by the same laser. Patterning is desirable in many cases for example in order to be able to contact a certain flake having a well-defined shape for further measurements. Figure 3A shows a confocal image of a typical exfoliated flake imaged by upconversion fluorescence using pulsed excitation at 780 nm wavelength. It consists of a large single layer which is however not suitable for contacting since

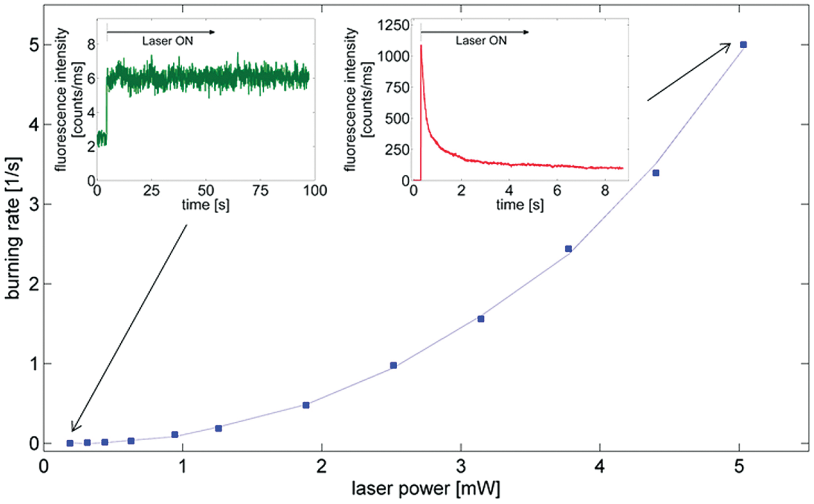


**Figure 2. Rate of burning as a function of laser power. In the imaging regime below 1 mW graphene is imaged without damage. However, graphene is efficiently removed using higher laser power. The left inset shows the time trace of the upconversion intensity for $P = 0.2$ mW. No damaged is inflicted even after 100 s. The right inset shows the efficient burning of graphene observed by the rapid decrease of the upconversion intensity. The laser power is measured at the input of the objective (0.95 NA). The blue line serves as a guide to the eye.**

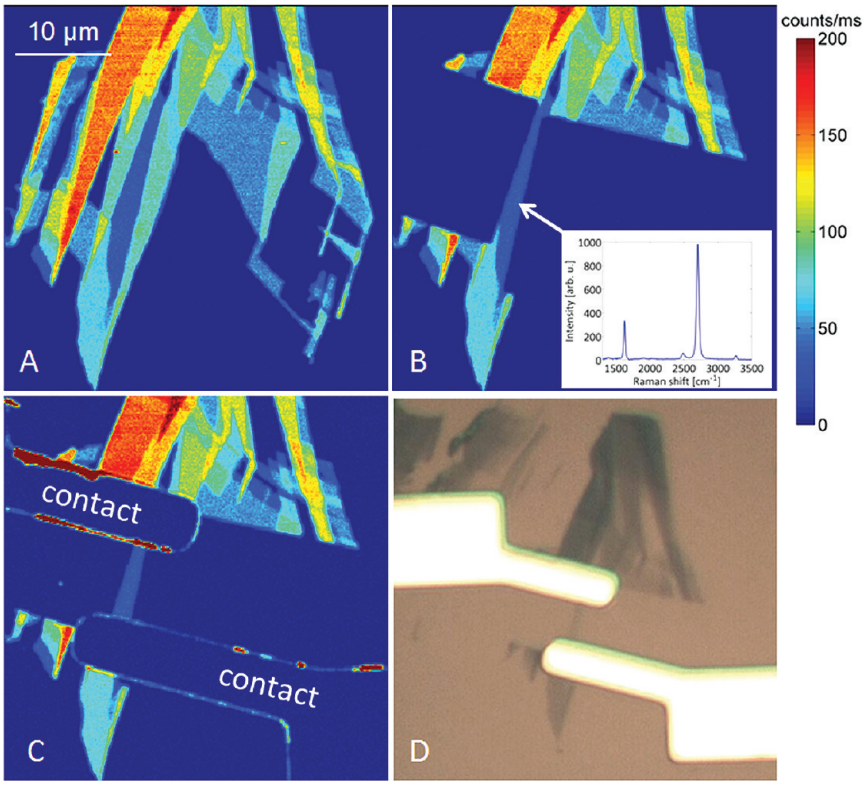


**Figure 3. (A) Typical flake imaged by upconversion luminescence to identify the exact shape and the number of layers. The single layer part in the center of the flake is surrounded by thicker parts and can therefore not be contacted as is. (B) Same flake after fully removing specific areas to make the remaining single layer suitable for contacting. The inset shows the Raman spectrum of the remaining part. The absence of the Raman D-line confirms the noninvasive nature of the shaping method. (C) Same flake after applying the metal contacts. The contours of the contacts can be seen on the top left and bottom right. (D) Widefield microscope image of the same sample.**

other parts of the flake would shortcut the contacts. However, by increasing the IR-laser intensity by roughly 1 order of magnitude it is possible to completely remove certain parts by laser etching without damaging the remaining flakes (see Figure 3B). Compared to other methods like catalytic hydrogenation[17] or plasma etching,[1,9] this way of shaping graphene has several advantages. First, because of

the absence of any chemicals contaminations or damage to the remaining flake are avoided. Second, since shaping and imaging are done *in situ* in the same confocal microscope it is not only convenient and fast but can also be done with high precision and accuracy. To further contact the flake in Figure 3, it was again imaged after applying a positive tone photoresist. It is worth noting that imaging the flake by upconversion does not expose the photoresist since low laser intensity is required for visualizing graphene. The desired parts of the photoresist were subsequently exposed *in situ* in the same confocal microscope by changing the excitation to a blue-ray laser diode ($\lambda$ = 405 nm). After development of the photoresist the contacts were applied by evaporation of titanium and gold and subsequent lift-off in acetone. Figure 3C shows a confocal image of the flake with the contours of the contacts in the top left and bottom right. The contacts are now only connected by the single layer and are not shortcut by other parts of the flake. The Raman spectrum of the remaining single layer taken after laser etching and contacting (see inset of Figure 3 B) is identical with the one of pristine graphene. The absence of the defect induced D-line confirms the noninvasive nature of the whole process including imaging, laser etching, and contacting the flake.

The resolution of shaping graphene as mentioned above is limited by the size of the confocal spot which is given by the Abbe-limit to be roughly $^{\lambda}/_{2} \approx 400$ nm. However, by introducing phase-shifting tilted optical flat or 2D vortex phase plates the laser beam profile can be shaped as shown in the insets of Figure 4C and Figure 5A. Since burning only occurs in the bright rim of the beam where the laser intensity exceeds a certain threshold, but not in the central node this increases the resolution considerably. By producing a donut-shaped laser profile as used for example for STED microscopy[18] it is possible to create round graphene dots with sizes well beyond diffraction limit. Figure 4 panels A and B show confocal and AFM images of a graphene layer after being exposed to the donut-shaped laser beam of different intensities. The size of the central dark spot of the laser beam profile is inversely proportional to the square root of the laser intensity. The size of the remaining graphene dot can therefore be controlled simply by changing the laser intensity. Figure 4C shows the dependence of the diameter of the graphene dots as a function of applied laser intensity following the described behavior.

Besides writing graphene dots by a 2D shaped laser beam ($TEM_{01*}$ Laguerre-Gaussian mode) it is also possible to write graphene nanoribbons by a 1D-shaped laser profile ($TEM_{10}$ Hermite-Gaussian mode). By creating a dark line in the center of the laser beam profile as shown in the inset of Figure 5 A and moving the laser across the flake parallel to the dark line, ribbons with

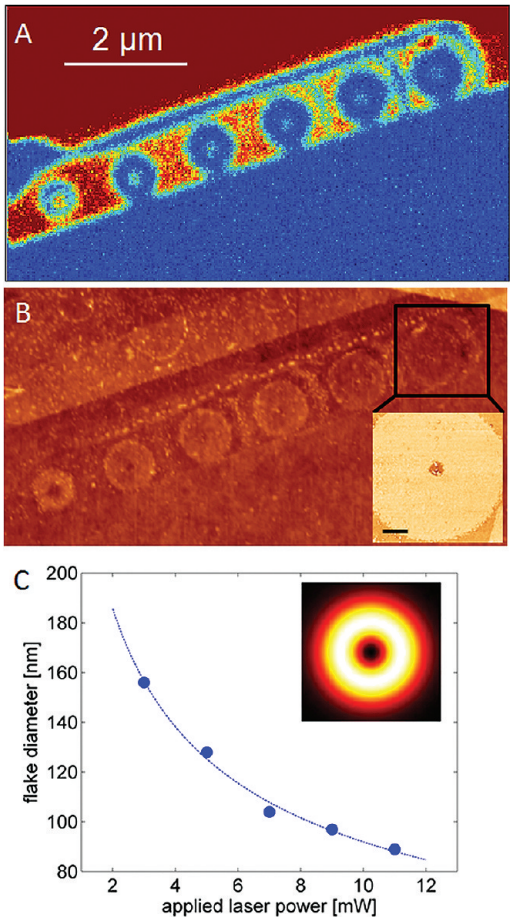


**Figure 4. Shaping graphene beyond diffraction limit. (A) Confocal upconversion image of a graphene flake after exposure to a donut-shaped laser beam using different laser intensities. (B) AFM image of the same flake showing dots of different size. The inset shows a close-up of the smallest dot. The scale bar is 200 nm. (C) Graphene dot diameter as a function of applied laser intensity. The inset shows schematically the laser beam profile.**

sizes smaller than the diffraction limit can be written. The precise size of the nanoribbons can again be controlled by changing the laser intensity. Alternatively, one can further reduce the width of the GNRs by keeping the laser intensity constant and scanning across the flake twice with a certain shift between the two cuts perpendicular to the dark central line of the laser beam. Figure 5A shows an exfoliated flake on $SiO_2$ substrate with a single layer part in the center. Applying several cuts in the way described above results in GNRs of different width as shown in Figure 4B–D (the white arrows indicate the GNRs). In this case, the spacing between two parallel $TEM_{10}$-laser cuts was varied from 200 to 400 nm. AFM measurements (Figure 5D) reveal that this spacing is directly related to the resulting width of the GNRs which is also shown in Figure 6E (the apex radius of the AFM tip of 10 nm has been taken into account by subtracting 20 nm from the width extracted from the raw data). Furthermore, Figure 5I shows that the upconversion intensity

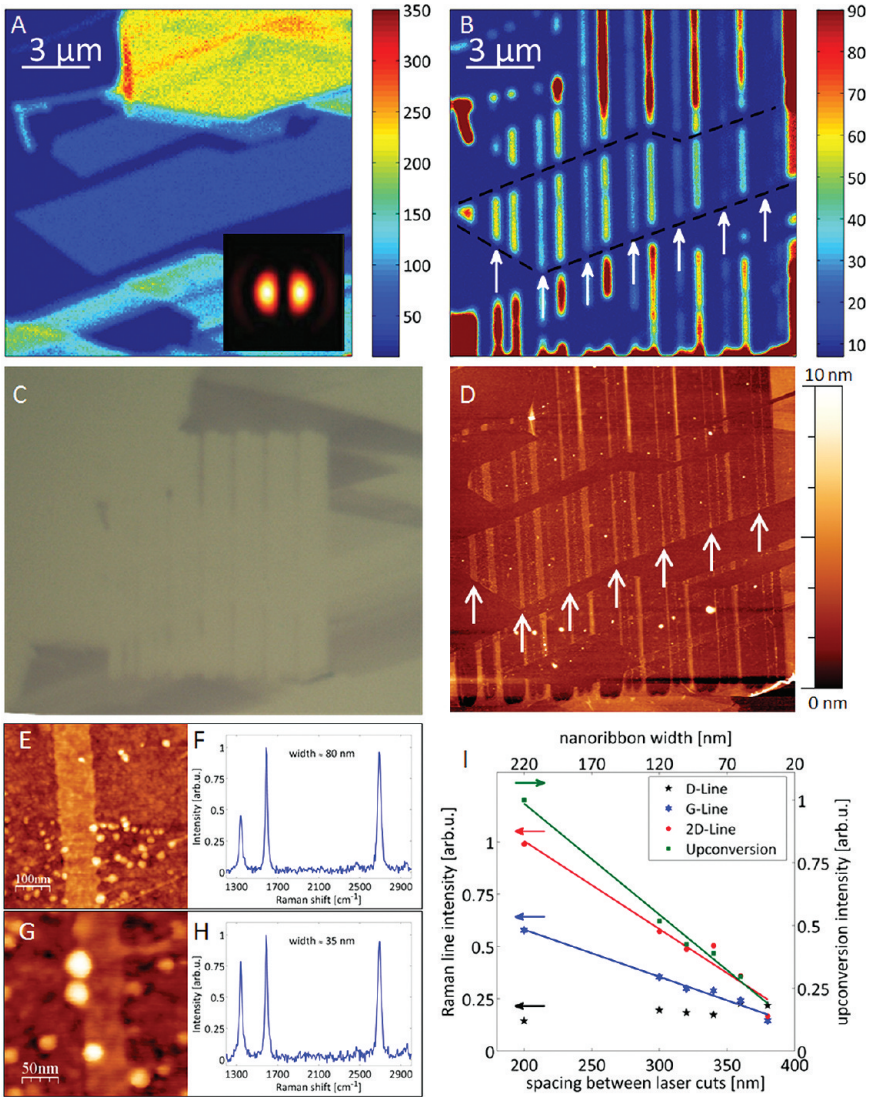


**Figure 5. Shaping graphene beyond diffraction limit. (A) Confocal upconversion image of an exfoliated flake with a single layer graphene in the center. The inset shows schematically the $TEM_{10}$ laser beam profile used for shaping. (B) The same flake after exposure to 1D-shaped laser beam. The resulting GNRs are indicated by white arrows and were written with different spacing between to parallel cuts. The color scale has been adjusted to show the nanosized graphene structures. (C and D) Widefield microscopy and AFM image of the same flake after shaping. (E and F) AFM image and Raman spectrum of a ribbon of 80 nm width. The upper and lower parts in panel E show a double and single layer, respectively. The Raman spectrum (F) has been taken on the single layer part. (G and H) AFM image of a GNR of 35 nm width along with its Raman spectrum. (I) Intensities of the Raman D, G, and 2D lines and the upconversion intensity as a function of the spacing between the two parallel laser cuts which is directly related to the resulting GNR width.**

emitted from each GNR depends linearly on the spacing between the laser cuts and can therefore be used as a measure of its width which will be discussed in more detail below.

The widefield microscopy image (Figure 5C) clearly shows that graphene is completely removed by the laser. However, AFM measurements (Figure 5D) reveal that small dots of 1−3 nm in height remain between the graphene stripes. Interestingly, this is only the case when burning single layer graphene (lower part of Figure 5E). In case of double layers the trenches between the ribbons are much cleaner (upper part of Figure 5E). We suggest that because of the high temperatures graphene might transform into another carbon allotrope (like for example fullerenes) and that this transition is somewhat hindered in the case of double layers. However, even in case of single layered graphene the resulting nanoribbon can be considered almost clean since there are only about 15 dots of less than 3 nm in size in a 250× 250 $nm^2$ scan (see Figure 5G). The fact that those dots look much bigger in the AFM scan results from 20 nm diameter of the AFM tip apex.

To further characterize the quality of the GNRs, Raman spectra have been recorded for each nanoribbon. The laser polarization vector was set along the ribbons. Figure 5I shows the intensity of the three dominant Raman features (D-line at 1350 $cm^{-1}$, G-line

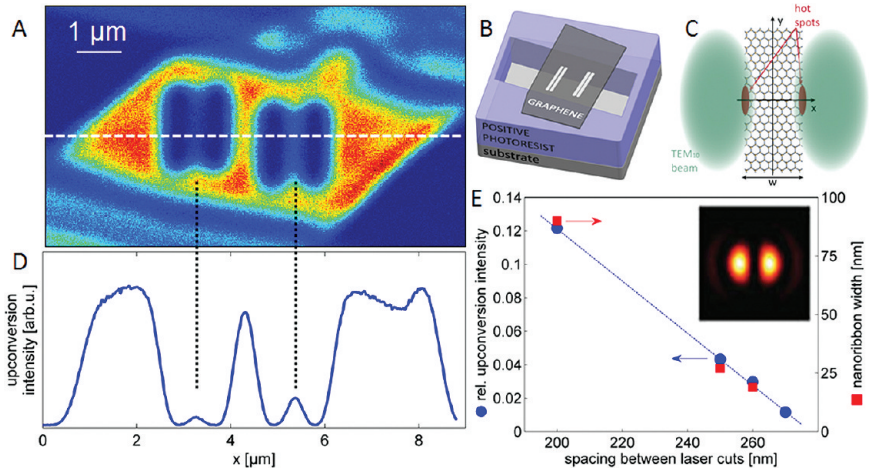


**Figure 6. Freely suspended graphene nanoribbons: (A) upconversion image of two freely suspended graphene nanoribbons with a width of 42 nm (left) and 143 nm (right); (B) schematic drawing of the sample geometry; (C) schematic drawing of burning graphene by $TEM_{10}$ laser beam; (D) intensity line scan across the white line used to determine the width of the GNRs based on their relative upconversion intensity; (E) reference sample of GNRs on $SiO_2$ substrate. Characterizing the sample both optically and by AFM yields a linear relationship between the upconversion intensity (normalized to the bulk graphene value) and the corresponding width of the GNRs. This relationship is further used to determine the width of freely suspended GNRs.**

at 1580 $cm^{-1}$ and 2D-line at 2700 $cm^{-1}$) as a function of the spacing between laser cuts and the resulting nanoribbon width. The intensities of the G- and 2D-line directly depend on the size of the irradiated graphene area.[19] Since the width of the GNRs is much smaller than the diffraction limited laser spot, the G- and 2D-line intensity is expected to be directly proportional to the width of the nanoribbons. This can in fact be observed for the GNRs under study as shown in Figure 5I. The D-line intensity, however, is not sensitive to the amount of $sp^2$-bond carbon but to the amount of structural disorder. In graphene nanoribbons, the D-line can either arise from the edge depending on its shape and roughness[20] or it can originate from defects within the bulk material.[19] In the case of the latter, the D-line intensity is expected to be proportional to the GNR width. However, the fact that, in our case, the D-line intensity does not significantly depend on the GNR width (see black stars in Figure 5I) evidence that almost no observable bulk disorder is introduced during the laser cutting process. The observed D-line intensity is therefore considered to predominantly originate from the edge of the GNR. Comparison of the Raman spectra taken for 80 and 35 nm wide GNRs produced by reactive ion etching and our laser etching technique (Figure 5E–H and Figure 2 of work 21) shows that the D/G-line ratio is improved by a factor of 3 in the case of laser-written GNRs. To us, this means, that besides their high structural quality within the bulk, laser written graphene nanoribbons also exhibit high quality edges.

To check that the GNRs are still conductive, the ends of a nanoribbon have been contacted in the way described above. Since those specific experiments were performed on glass substrates it was not possible to apply gate voltage; hence, mobility could not be extracted. However, a GNR 120 nm wide and 10 $\mu$m long shows a resistance of 30 kΩ which is in agreement with the values reported in literature.[9]

Besides having nanoribbons on a substrate produced in the way described above it is crucial for many experiments to have nanoribbons which are freely suspended to avoid interactions with the substrate.[11] To our knowledge, so far only one method of producing such structures has been reported.[22] This procedure, however, requires a specialized helium ion microscope particularly engineered for lithography purposes. However, the much simpler laser-based technique described above can be applied to freely suspended graphene flakes resulting in freely suspended GNRs. In our experiments the freely suspended graphene and GNRs were produced in the following way. After applying a positive tone photoresist to any arbitrary substrate graphene was attached on top by mechanical exfoliation. By imaging with upconversion fluorescence flakes could be identified without exposing the resist. After finding a suitable flake a horizontal trench across the graphene was written into the resist and subsequently the sample was developed. This results in a graphene flake freely suspended which can then be cut into nanoribbons following the procedure described above. In general, shaping graphene into GNRs in the way described above can also be applied to graphene freely suspended by any other technique. Figure 6B shows a schematic drawing of the sample. In this study, the photoresist was exposed by two-photon absorption of 780 nm wavelength rather than by UV exposure.[23–25] The laser intensity was adjusted to be below the burning threshold for graphene, but high enough to expose the photoresist.

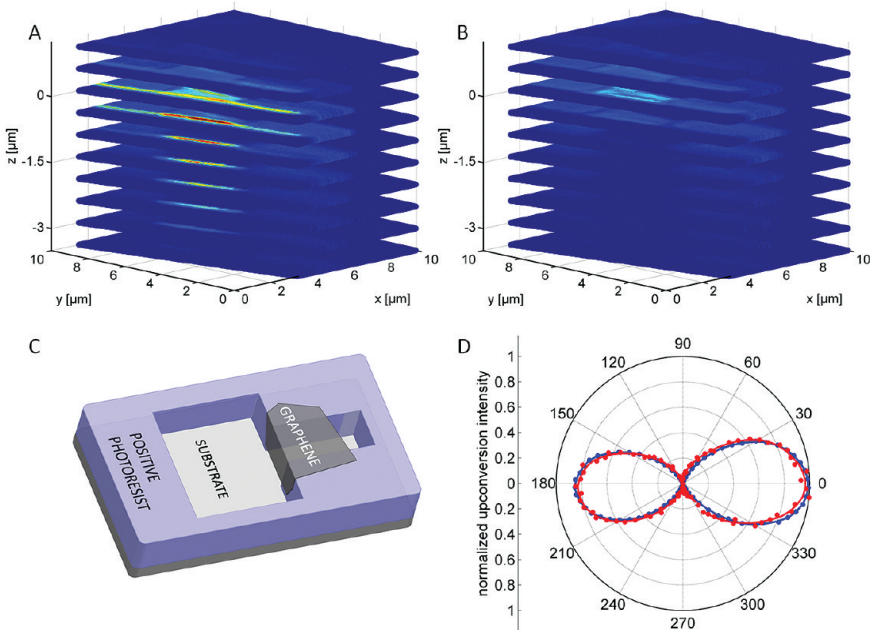


**Figure 7. (A) 3D confocal scan of freely hanging graphene with the polarization vector parallel to the vertically hanging flake. (B) The same scan but with the polarization vector being perpendicular to the hanging flake. The surface of the photoresist is at $z \approx 0\ \mu$m together with the horizontal part of the flake. The vertical part of the flake is hanging down until $z \approx -2.5\ \mu$m. The part from $y \approx 3$ to $6\ \mu$m is freely hanging. (C) Schematic drawing of the sample geometry. The photoresist has been exposed in a T-shaped trench resulting in the flake hanging vertically and freely between the walls. (D) Polar plot of the upconversion intensity as a function of the angle between the excitation laser polarization and the flake surface in case of graphene (blue). The same anisotropy for carbon nanotubes with the angle between the laser polarization and the axes of the nanotube is shown in red. The difference in maximum intensity at 0° and 180° is a result of slowly damaging the graphene and carbon nanotube due to long laser irradiation to a single point (several tens of minutes).**

This enables us to write trenches with high accuracy and straight walls even for thick photoresist layers. Figure 6A shows a freely suspended graphene flake with two nanoribbons written inside by scanning the 1D-shaped laser beam twice in the way described above. The difference in the laser shift for the two GNRs and, consequently, the expected width difference was 100 nm. Since those nanoribbons are now freely suspended, their size can not be measured by AFM. However, the width can be determined by comparing the upconversion intensity of the left and right ribbon ($I_{left}$, $I_{right}$) with that of the bulk graphene. The reference can be taken from the GNRs on a substrate for which direct comparison between the known AFM width and the upconversion intensity is possible. For this, a sample with graphene on a $SiO_2$ substrate has been prepared and characterized under the same experimental conditions (*i.e.*, same pinhole size, identical alignment, *etc.*). Figure 6E shows the relative upconversion intensity as a function of the spacing between the two parallel laser cuts together with the width of the GNRs as determined by AFM. Again, a linear relationship between the GNR width and the relative upconversion intensity can be observed. In the following, this relationship is used to determine the width of freely suspended GNRs. The upconversion intensity along the white line across the two freely suspended nanoribbons is shown in Figure 6D. Comparing this with Figure 6E, the width of the two nanoribbons was determined to be 42 nm (left) and 143 nm (right). Again, the difference in width is in good agreement with the difference between the spacing of the two cuts for each nanoribbon. By knowing this, one can also extract the width by simply comparing the ratio of the two intensities $I_{left}/I_{right}$ with a change in width by 100 nm: $I_{left}/I_{right} = d_{left}/(d_{left} + 100\ \text{nm})$. This values are also in good agreement with the ones from above.

To present more insight into how nanoshaping of graphene works, let us consider a simplified semiempirical model of thermal oxidation of freely suspended graphene induced by a $TEM_{10}$-shaped laser pulse. Graphene is known to have the highest thermal conductivity among all the materials. Thus, the local heating by the laser can be efficiently diminished by heat transport along the flake. Therefore, to estimate the minimum size of the feature that can be obtained by laser burning, one has to take into account heat transport dynamics. We assume that the dark stripe of the laser beam is centered on an infinitely long graphene nanoribbon of width $w$ directed along $y$-axis (see Figure 6C). Obviously, the heat generated by the laser beam can be dissipated outside of the hot region only through the nanoribbon itself whose ends at $y = \pm\infty$ are assumed to be at ambient temperature. The lateral beam profile along with its temporal dependence is described by the following intensity

distribution:

$$I_{las} = I_0 \frac{x^2}{a^2} \exp\left(-\frac{x^2+y^2}{a^2}\right) \exp\left(-\frac{t^2}{\tau^2}\right) \quad (1)$$

where $a$ is the size of the beam waist and $\tau$ is the laser pulse duration. Under our experimental conditions $a$ is close to quarter of the laser wavelength and can be estimated as 200−300 nm. The amount of light absorbed locally by the flake is $\alpha I_{las}$ where $\alpha$ is the absorption coefficient of graphene known to be ~2.3%. Those parts of the flake whose temperature is below the oxidation onset temperature (known to be around 800 K[26]) at all times will not burn. Thus, the steady-state situation is reached (narrowing of the nanoribbon stops) once the maximum temperature of the hottest spot of the nanoribbon is just below 800 K at all times. There are several characteristic time scales involved in heat dynamics: (1) the duration of the heating laser pulse $\tau$, (2) the heat transport time across the nanoribbon $\tau_w$, (3) the time $\tau_a$ required to transport heat along the nanoribbon by the laser beam size, and (4) laser pulse repetition period $T_p$. In our case, the $\tau \approx 100$ fs while $T_p = 13$ ns. Thus, the heat diffusion length in between the two subsequent pulses can be estimated as $L_p = (T_p\alpha)^{1/2} = 4\ \mu$m. Since $L_p \gg a$, it is safe to assume that in between the two laser pulses the nanoribbon cools down completely. The other two time scales can be estimated as $\tau_w = w^2/\alpha$ and $\tau_a = a^2/\alpha$ where $\alpha$ is the thermal diffusivity of graphene. We assume that its value is close to that of pyrolytic graphite known to be $1.1 \times 10^{-3}$ m$^2$/s at room temperature.[27] Thus, we obtain $\tau_a = 30$ ps for $a =$ 200 nm meaning that heat transfer along the nanoribbon does not occur during the laser pulse. If $w \ll a$, the heat transport across the nanoribbon happens much faster. Two regimes can be distinguished. In the first regime, when the pulse duration is longer than $\tau_w$, the temperature is constant across the nanoribbon. In the second regime, when $\tau < \tau_w$, there are two hottest spots on the nanoribbon at the points $y = 0$ and $x = \pm w/2$. This regime represents local laser heating and burning. Therefore, limiting size of the nanoribbon can be estimated as $w = (\alpha\tau)^{1/2} \approx 10$ nm. At the same time, the quality of the nanoribbon edges is determined by how strict the oxidation threshold is.

In general, so far, all optical studies on graphene have been performed with the optical access perpendicular to the flake. In that way the laser polarization vector can only be rotated in-plane and the laser $\vec{k}$-vector is always perpendicular to the flake. Some studies have already been performed by rotating the polarization vector in-plane where an anisotropy of the polarization dependence of the 2D Raman line could be observed.[28] However, so far it was not possible to study the out-of-plane anisotropy of any optical effects in graphene or to excite graphene optically with the laser $\vec{k}$-vector parallel to the flake. In the following we demonstrate a way of freely hanging graphene vertically (*i.e.*, perpendicular to the substrate) which can afterward be imaged in 3D. Like in the case of freely suspended nanoribbons, graphene was applied on top of a positive tone photoresist. After identifying a suitable flake with upconverted fluorescence, a T-shaped trench was written into the resist so that during the development process a part of the flake can bend toward the bottom of the trench while the rest remains parallel to the substrate. The vertically hanging part will then be supported on the two vertical walls of the trench leaving the central part freely hanging. A schematic drawing of the sample geometry is shown in Figure 7C.

For creating these kind of 3D structures it is again crucial to expose the photoresist by two-photon absorption to ensure straight and smooth side walls. After development, the flake was visualized by scanning several slices in $z$ with a spacing of 500 nm to create a 3D image as shown in Figure 7A. Here, the surface of the photoresist is at $z \approx 0\ \mu$m together with the horizontal part of the flake. From there, the rest of the flake is hanging down vertically until $z \approx -2.5\ \mu$m freely suspended between $y \approx 3$ and 6 $\mu$m. For this scan, the laser polarization vector was set to be parallel to the vertical part of the flake resulting in a maximum of upconversion fluorescence. Turning the polarization by 90° results in a minimum of the upconversion intensity of the vertical part while the intensity of the horizontal part remains unchanged (see Figure 7B). Figure 7D shows the upconverted intensity as a function of the relative angle between the flake and the polarization vector. A similar behavior was found for Raman G-line.[29] It is known from the band structure of graphene that for the polarization vector parallel to the flake the $\pi \rightarrow \pi^*$ and $\sigma \rightarrow \sigma^*$ transitions are allowed.[30] These transitions give rise to electronic excitations and, consequently, to upconverted fluorescence. If the polarization vector is perpendicular to the flake, only the $\pi \rightarrow \sigma^*$ and $\sigma \rightarrow \pi^*$ transitions are allowed. However, the energies of those transitions lie deep in the UV.[31] Once the polarization vector is perpendicular to the flake electrons cannot be promoted from the valence band into the conduction band and, therefore, no fluorescence can be excited. A similar polarization dependence of the upconversion was found for single-walled carbon nanotubes (see red line in Figure 7D). However, for some nanotubes the upconversion intensity does not completely vanish in the case of perpendicular polarization. This might be due to the difference between semiconducting and metallic carbon nanotubes but is, however, not studied in detail yet. Finally, for freely suspended GNRs produced in the way described above no anisotropy could be observed. This proves that the GNRs are still flat and did not curl up on the sides.

## CONCLUSIONS

We demonstrated a laser-based way of producing graphene nanodots and nanoribbons. We show that this purely optical technique can be used to write GNRs of as narrow as 20 nm wide and can be applied even to freely suspended graphene. In principle, STED-like techniques have no limitation in terms of spatial resolution and, therefore, GNRs of arbitrarily small width could be produced. However, further studies including numerical simulations of the local chemical reaction responsible for burning have to be performed to clarify the ultimate spatial precision of this patterning technique. Potentially, laser burning of graphene can be used for producing graphene with edges well-defined on the atomic scale (for example, zigzag or armchair) over large distances. Finally, we managed to freely suspend graphene vertically (perpendicular to the substrate) and image it in 3D. We demonstrate the anisotropy of the upconverted luminescence as a function of the relative angle between the laser polarization and the surface of the vertically hanging graphene. Further experiments on a single atomic layer viewed from the side might reveal new interesting optical properties of graphene. Those might include detection of optically excited plasmons under the condition of incident wave vector being parallel to the flake, studying out-of-plane mechanical vibrations of freely hanging graphene, *etc*.

## EXPERIMENTAL SECTION

For this study, graphene flakes were prepared by mechanical exfoliation of highly oriented pyrolytic graphite (HOPG, Advanced Ceramics)[1,2] and subsequently transferred to suitable substrates. The two main substrates used in this study were glass (150 $\mu$m thickness) and $Si/SiO_2$ (300 nm of oxide layer thickness). Other substrates like $Si/Si_3N_4$ (100 nm of nitride layer thickness), diamond, sapphire, and yttrium aluminum garnet have also been tested showing similar results. The output of a mode-locked Ti:Sapphire laser was used for luminescence excitation and two-photon exposure of the photoresist after being passed through a short piece of a single-mode photonic crystal fiber to ensure its Gaussian beam profile. The excitation wavelength was kept at 780 nm with a spectral width of 20 nm and a total pulse length of 100 fs at a repetition rate of 76 MHz. Confocal measurements as well as optical lithography were carried out in a home-built confocal microscope. The parallel laser beam was focused onto the sample by using either a 1.3 NA oil immersion objective or a 0.95 NA air objective resulting in a diffraction limited spot. The sample was mounted on a 3D nanopositioning stage. The fluorescence light was separated from the laser light by a polarizing beam splitter cube and sent through a 50 $\mu$m pinhole for spatial filtering which allows only the in-focus portion of the light to be detected. Images were recorded by an avalanche photo diode (APD) with the light spectrally filtered by a 680 nm short-pass filter. The laser used for subdiffraction limited shaping of graphene was a diode pumped solid-state mode-locked laser at 532 nm wavelength, 10 ps pulse width and 76 MHz repetition rate. Raman measurements were carried out by using a continuos-wave laser at 532 nm wavelength. The excitation wavelength was blocked by a 545 nm long-pass filter. The positive tone photoresist used here was AZ 9260 (MicroChemicals) together with developer AZ 400K (MicroChemicals) diluted 1:3 (development time 20 min.). The resist was spin-coated on plasma-cleaned substrates resulting in a film thickness of roughly 10 $\mu$m and prebaked for 3 min at 110 °C.

*Acknowledgment.* We acknowledge Petr Siyushev, Fedor Jelezko, Gopalakrishnan Balasubramanian, and Jurgen Smet for useful discussions and support. Financial support was provided by the Baden-Württemberg Stiftung *via* the Kompetenznetz Funktionelle Nanostrukturen.

## REFERENCES AND NOTES

1. Novoselov, K. S.; Geim, A. K.; Morozov, S. V.; Jiang, D.; Katsnelson, M. I.; Grigorieva, I. V.; Dubonos, S. V.; Firsov, A. A. Two-Dimensional Gas of Massless Dirac Fermions in Graphene. *Nature* **2005**, *438*, 197–200.
2. Novoselov, K. S.; Geim, A. K.; Morozov, S. V.; Jiang, D.; Zhang, Y.; Dubonos, S. V.; Grigorieva, I. V.; Firsov, A. A. Electric Field Effect in Atomically Thin Carbon Films. *Science* **2004**, *306*, 666–669.
3. Geim, A. K.; Novoselov, K. S. The Rise of Graphene. *Nat. Mater.* **2007**, *6*, 183–191.
4. Zhang, Y.; Tan, Y.-W.; Stormer, H. L.; Kim, P. Experimental Observation of the Quantum Hall Effect and Berry's Phase in Graphene. *Nature* **2005**, *438*, 201–204.
5. Fujita, M.; Wakabayashi, K.; Nakada, K.; Kusakabe, K. Peculiar Localized State at Zigzag Graphite Edge. *J. Phys. Soc. Jpn.* **1996**, *65*, 1920–1923.
6. Nakada, K.; Fujita, M.; Dresselhaus, G.; Dresselhaus, M. S. Edge State in Graphene Ribbons: Nanometer Size Effect and Edge Shape Dependence. *Phys. Rev. B* **1996**, *54*, 17954–17961.
7. Wakabayashi, K.; Fujita, M.; Ajiki, H.; Sigrist, M. Electronic and Magnetic Properties of Nanographite Ribbons. *Phys. Rev. B* **1999**, *59*, 8271–8282.
8. Barone, V.; Hod, O.; Scuseria, G. E. Electronic Structure and Stability of Semiconducting Graphene Nanoribbons. *Nano Lett.* **2006**, *6*, 2748–2754.
9. Han, M. Y.; Özyilmaz, B.; Zhang, Y.; Kim, P. Energy Band-Gap Engineering of Graphene Nanoribbons. *Phys. Rev. Lett.* **2007**, *98*, 206805.
10. Chen, Z.; Lin, Y.-M.; Rooks, M. J.; Avouris, P. Graphene Nanoribbon Electronics. *Phys. E* **2007**, *40*, 228–232.
11. Meyer, J. C.; Geim, A. K.; Katsnelson, M. I.; Novoselov, K. S.; Booth, T. J.; Roth, S. The Structure of Suspended Graphene Sheets. *Nature* **2007**, *446*, 60–63.
12. Bolotin, K.; Sikes, K.; Jiang, Z.; Klima, M.; Fudenberg, G.; Hone, J. Ultrahigh Electron Mobility in Suspended Graphene. *Solid State Commun.* **2008**, *146*, 351–355.
13. Berger, C.; Song, Z.; Li, X.; Wu, X.; Brown, N.; Naud, C.; Mayou, D.; Li, T.; Hass, J.; Marchenkov, A. N.; ; *et al.* Electronic Confinement and Coherence in Patterned Epitaxial Graphene. *Science* **2006**, *312*, 1191–1196.
14. Stöhr, R. J.; Kolesov, R.; Pflaum, J.; Wrachtrup, J. Fluorescence of Laser-Created Electron-Hole Plasma in Graphene. *Phys. Rev. B* **2010**, *82*, 121408.
15. Liu, W.-T.; Wu, S. W.; Schuck, P. J.; Salmeron, M.; Shen, Y. R.; Wang, F. Nonlinear Broadband Photoluminescence of Graphene Induced by Femtosecond Laser Irradiation. *Phys. Rev. B* **2010**, *82*, 081408.
16. Balandin, A. A.; Ghosh, S.; Bao, W.; Calizo, I.; Teweldebrhan, D.; Miao, F.; Lau, C. N. Superior Thermal Conductivity of Single-Layer Graphene. *Nano Lett.* **2008**, *8*, 902–907.
17. Datta, S. S.; Strachan, D. R.; Khamis, S. M.; Johnson, A. T. C. Crystallographic Etching of Few-Layer Graphene. *Nano Lett.* **2008**, *8*, 1912–1915.

18. Rittweger, E.; Han, K. Y.; Irvine, S. E.; Eggeling, C.; Hell, S. W. STED Microscopy Reveals Crystal Colour Centres with Nanometric Resolution. *Nat Photon* **2009**, *3*, 144–147.
19. Malard, L.; Pimenta, M.; Dresselhaus, G.; Dresselhaus, M. Raman Spectroscopy in Graphene. *Phys. Rep.* **2009**, *473*, 51–87.
20. Krauss, B.; Nemes-Incze, P.; Skakalova, V.; Biro, L. P.; Klitzing, K. v.; Smet, J. H. Raman Scattering at Pure Graphene Zigzag Edges. *Nano Lett.* **2010**, *10*, 4544–4548.
21. Bischoff, D.; Güttinger, J.; Dröscher, S.; Ihn, T.; Ensslin, K.; Stampfer, C. Raman Spectroscopy on Etched Graphene Nanoribbons. *J. Appl. Phys.* **2011**, *109*, 073710.
22. Bell, D. C.; Lemme, M. C.; Stern, L. A.; Williams, J. R.; Marcus, C. M. Precision Cutting and Patterning of Graphene with Helium Ions. *Nanotechnology* **2009**, *20*, 455301.
23. Witzgall, G.; Vrijen, R.; Yablonovitch, E.; Doan, V.; Schwartz, B. J. Single-Shot Two-Photon Exposure of Commercial Photoresist for the Production of Three-Dimensional Structures. *Opt. Lett.* **1998**, *23*, 1745–1747.
24. Gansel, J. K.; Thiel, M.; Rill, M. S.; Decker, M.; Bade, K.; Saile, V.; von Freymann, G.; Linden, S.; Wegener, M. Gold Helix Photonic Metamaterial as Broadband Circular Polarizer. *Science* **2009**, *325*, 1513–1515.
25. Zhang, Y.-L.; Chen, Q.-D.; Xia, H.; Sun, H.-B. Designable 3D Nanofabrication by Femtosecond Laser Direct Writing. *Nano Today* **2010**, *5*, 435–448.
26. Badenhorst, H.; Rand, B.; Focke, W. Modelling of Natural Graphite Oxidation Using Thermal Analysis Techniques. *J. Therm. Anal. Calorim.* **2010**, *99*, 211–228.
27. Kato, H.; Baba, T.; Okaji, M. Anisotropic Thermal-Diffusivity Measurements by a New Laser-Spot-Heating Technique. *Meas. Sci. Technol.* **2001**, *12*, 2074.
28. Yoon, D.; Moon, H.; Son, Y.-W.; Samsonidze, G.; Park, B. H.; Kim, J. B.; Lee, Y.; Cheong, H. Strong Polarization Dependence of Double-Resonant Raman Intensities in Graphene. *Nano Lett.* **2008**, *8*, 4270–4274.
29. In our experiment we observed anti-Stokes Raman G-line instead of the Stokes line because of high fluorescence background from the photoresist.
30. Klucker, R.; Skibowski, M.; Steinmann, W. Anisotropy in the Optical Transitions from the $\pi$ and $\sigma$ Valence Bands of Graphite. *Phys. Status Solidi (b)* **1974**, *65*, 703–710.
31. Trevisanutto, P. E.; Holzmann, M.; Côté, M.; Olevano, V. *Ab Initio* High-Energy Excitonic Effects in Graphite and Graphene. *Phys. Rev. B* **2010**, *81*, 121405.